MXene Incorporated Polymeric Hybrids for Stiffness Modulation in Printed Adaptive Surfaces

*Ankit[1,2], Febby Krisnadi[1], Shreyas Pethe[1], Kwang Jen Ryan Lim[1], Mohit Rameshchandra Kulkarni[1], Dino Accoto[2], Nripan Mathews[1,3]**

[1] School of Materials Science and Engineering
Nanyang Technological University, Singapore 639798.

[2] Robotics Research Centre, School of Mechanical and Aerospace Engineering
Nanyang Technological University, Singapore 639798.

[3] Energy Research Institute @ NTU (ERI@N)
Nanyang Technological University, Singapore 637553.

*Corresponding author: Nripan@ntu.edu.sg

Keywords
Soft robotics, Rigidity modulation, MXenes, Dielectric elastomer actuators, Adaptive surfaces

Abstract

Polymeric materials systems developed for actuators and human-machine interfaces suffer from limitations associated with effective force output due to their low mechanical modulus. New material solutions which can provide intrinsic multi-modal responses are needed to reversibly modulate rigidity; to be flexible, stretchable and bendable one moment, and to be rigid, able to bear load and resist deformation at another moment. Thermally modulated phase transition materials are promising for modulation of mechanical properties; however, they have not been explored for electrically driven shape morphing and responsive surfaces which requires favourable electrical properties too. Polymers like polyethylene glycol (PEG) allows for low melting point (56°C) and high dielectric constant (10), however they are limited by slow crystallisation kinetics and large temperature window. We architect an MXene incorporated PEG-water hybrid which allows for both reduction in melting point and rapid heterogeneous nucleation, which in turn increases the crystallization point. Multimodal response is demonstrated via thermal and electrical input, resulting in modulation of 700 times in Young's modulus, 100 times in flexural modulus and 10 times in hardness as well as large actuation strains (~28%) at low electric fields (~0.7 V/μm). They can be printed to create hardness domains, allowing for local and programmable modulation. An all-printed haptic device with an array of 3x3 pixels has been demonstrated capable of independently varying the hardness values for each pixel.

1. Introduction

Tissues like animal muscles serve as an inspiration for investigating compliant and conformable polymeric systems for next generation human-machine interfaces and soft and wearable robotic applications. [1] Soft robotic system comprises of actuators, sensors and other stimuli responsive robotic elements fabricated from soft material systems.[2-5] These soft systems are expected to be superior in their manoeuvres in unstructured environments (including collaborating with humans) to perform delicate tasks. Utilization of soft materials has enabled actuators with high actuation strains, numerous flexible configurations, and superior mechanical compliance at human-machine interfaces.[6-9] However, these soft materials cannot emulate the dual behaviour of these natural systems. Biological systems can not only behave as adaptive force generators which can maintain their posture and absorb impacts but can also adjust the properties to perform tasks like weight-lifting, when required. [10,11] Utilization of contemporary compliant polymeric systems for performing motor tasks in soft robotics or force feedback in haptic systems, leads to a conspicuous anomaly. The maximum mechanical stress supported by a soft material is directly proportional to its Young's modulus. [12] So, even though the utilization of compliant elastomers for soft robotic and haptic applications enables fluidity, dexterity and impervious interactions with the surrounding environment, it does create an issue of low force output limiting their applicability. [12] A mechanism to modulate the mechanical properties is required to increase this force output when needed. Natural systems mitigate this challenge by demonstrating remarkable variations in their mechanical properties under different circumstances. These changes can be triggered by a variety of stimulus like temperature (transition of stiffness for byssal threads in mussels), moisture (abrupt loss of stiffness in hemicellulose, basic constituents of plants) and electrical signals (living tissues like muscle where the brain triggers the fibres to modulate their elastic rigidity). [11,13]

There is thus a need to develop material systems that can display environment-responsive manipulation and adapt to operational circumstances. These systems would enable development of dexterous mechanisms for conventional robotic applications like gripping, where it can handle delicate tasks and fragile objects, and then switch to heavy-lifting jobs on demand. Apart from traditional robotic applications like gripping, these systems could also facilitate human-machine interfaces which are able to accommodate free motion in one instance and can offer assistive mechanical work on the other. Several technologies like pneumatics, fluidics, magnetic fields, and electroactive polymers (EAPs) have been utilised to achieve actuation in soft polymeric systems. [6,14-18] Electrically driven soft actuators are especially attractive owing to their light-weight and compact design, high actuation strains and easier control via an electric field. [19-21] However, there is still a need to extend the rigidity modulation response of such systems to achieve circumstance specific compliance matching. New material solutions which can provide intrinsic multi-modal responses are needed to reversibly modulate rigidity; to be flexible, stretchable and bendable one moment, and to be rigid, able to bear load and resist deformation at another moment.

Material approaches for achieving variable stiffness include phase change materials (PCMs), electrorheological fluids (ERFs) and magnetorheological fluids (MRFs) and rely on application of heat or electromagnetic fields for altering the mechanical properties. [12,22] In the case of ERFs and MRFs, the electromagnetic field has to be continuously applied for maintaining the high modulus state, which is not necessarily the case in PCMs. PCMs like thermoplastics and low melting point alloys (LMPAs), with either low melting (T_m) or low glass transition temperatures (T_g), have been explored by researchers. [23-26] The change in the microstructure associated with such transitions lead to a variation in the Young's modulus and enables rigidity modulation. [12] However, in these prior reports, the variable stiffness systems are attached onto the actuation mechanism, with the two existing as separate systems. Hence, these material

stiffening approaches do not contribute directly to the actuation performance. Additionally, LMPAs such as eutectic gallium indium (EGaIn), galinstan & Field's metal raise cost concerns as they are very expensive metal eutectics, incorporating rare earth elements.

Herein, we architect a novel hybrid that responds to two external stimuli-electric field and temperature, to undergo transformations which can be temporally and spatially controlled. We identify polyethylene glycol (PEG), a semicrystalline polymer, as the phase change matrix. PEG can undergo thermally triggered phase transitions owing to its molecular structure, chain length and intramolecular bonding, for reversible modulation of mechanical properties and possess a high dielectric constant (necessary for electroactive applications) owing to the presence of end hydroxyl groups. We choose an appropriate molecular weight (2000) PEG matrix with a low melting point (~56℃), superior thermal stability, high mechanical strength and high dielectric constant (10). However, pristine PEG matrix has a broad temperature window between melting and crystallization (~ 30℃) which leads to sluggish cycle times. Hence, MXene incorporated PEG-water hybrids were architected to reduce the cycle times by more than half. Water interacts with PEG molecules via hydrogen bonding and results in reduction of melting point. MXene nanoflakes act as nucleating agents leading to rapid heterogeneous nucleation, which in turn increases the crystallization point. To the best of our knowledge, this is the first report of a PEG-water-MXene composite for reversible rigidity demonstrations. Hybrids with 700 times modulation in Young's modulus, 100 times change in flexural modulus and 10 times alteration in hardness were demonstrated. Owing to its ability to melt and solidify over several cycles, the composites demonstrate healing after suffering severe mechanical damage. Employing the hybrids as an electroactive matrix in a dielectric elastomer actuator (DEA) configuration, linear actuation strain of ~28% was achieved at significantly low electric field (~0.7 V/μm). This versatile material can be printed on to substrates to demonstrate hardness domains and engineer hardness gradients. We have

demonstrated enhanced haptic devices by augmenting hardness domains on top of electrically controlled surface deformations in thickness mode DEAs. Furthermore, capitalizing on the printing of Ag joule heaters and hardness domains, an all printed haptic communicator of 3x3 array of pixels has been demonstrated creating specific hardness gradients by actuation of individual devices.

2. Results and Discussion

2.1 Principle of Design and Choice of materials

Thermal modulation of mechanical properties requires polymers with low glass transition (T_g) or melting (T_m) temperatures where the application of temperature transforms it from a semi-crystalline state to a disordered amorphous state. Our approach focusses on capitalizing on this thermally triggered rearrangement for modulation on the force output. Video S1 showcases a scenario where the adaptive surfaces with embedded thermomechanical materials modify their mechanical properties upon thermal activation, and in doing so change the impact behaviour. When the material is in solid state, the colliding objects change their direction upon impact. However, upon melting the material, the objects hurtling towards the surface collide inelastically and come to a halt. Going beyond the thermal phase change, we seek to capitalize on electrically controlled shape morphing in the amorphous state (**Fig. 1A**). **Fig. 1A** presents the principle of design for the composite. In the semi-crystalline state or solid state of the polymer, the composite remains in rigid state and maintains its shape. Upon application on thermal stimulus, polymer melts and transitions to an amorphous state. Consequently, composite transitions to a soft state and becomes flexible. Furthermore, in the amorphous state of the polymer, an electrical stimulus can be applied to morph the shape of the composite. Our system consists of PEG (MW=2000) encapsulated in a polymer matrix. Lower molecular weight PEGs are viscous liquids at room temperature while higher molecular weight PEGs (> 2000) are flaky solids at room temperature that easily melt upon heating. [27]

Apart from LMPAs that are considered expensive and composed of rare earth elements like indium, the frequent choice of researchers for a low-temperature PCM has been paraffin wax. [24,28] Differential scanning calorimetry (DSC) (**Fig. 1B**) reveals similar melting points (T_m) for both PEG (~55℃) and paraffin wax (~59℃). However, a significant difference was observed in the solidification temperature for both materials, ~25℃ for PEG versus ~54℃ for wax. This large temperature window provides an operational period for actuation without the need of applying continuous thermal perturbation. On the other hand, wax has a very small temperature difference between melting and solidification, which leads to fast solidification process once heating was removed. Thermogravimetric analysis (TGA) of PEG and wax (**Fig. S1**) again revealed its superior thermal stability.

As our approach focusses on phase transition from solid to liquid state, the magnitude of rigidity modulation in the composites is determined by the mechanical strength of their constituent fillers in solid state. Uniaxial compression measurements provide information about the load bearing ability before failure for both the material systems. A steeper load-extension curve (**Fig. S2**) indicated a better load bearing ability for PEG, with smaller compression at similar load when compared to wax. Fracture for PEG-filled composite was observed at ~ 244 N (~0.58 mm compression) against ~40 N (~0.36 mm compression) observed in the case of wax, pointing to a significant difference in terms of compressive strength between both the materials. Dielectric spectroscopy reveals orders of magnitude higher dielectric constant (ε') for PEG compared to wax (**Fig. 1C** and **Fig. S3**), at lower frequencies. This difference between relative permittivity decreases with increasing frequency but PEG still maintains a significantly higher value than wax. ε' values for PEG were measured to be 142, 52, 22 and 10 at 1 Hz, 10 Hz, 100 Hz and 1 kHz, respectively. Paraffin wax, on the other hand, showed non-frequency dependant dielectric behaviour, with a stable ε' value (4.3-4.2) for all frequencies. The high dielectric constant of PEG is attributed to the presence of end hydroxyl

groups and the flexible oxyethylene chain of the molecule. [29,30] Presence of these ionic and dipole species present in the molecule lends PEG a highly frequency dependent permittivity behaviour (**Fig. 1C**). [29,30] The high dielectric constant of these materials indicates their suitability for devices employing the capacitive architecture, like field driven dielectric elastomer actuators (DEAs).

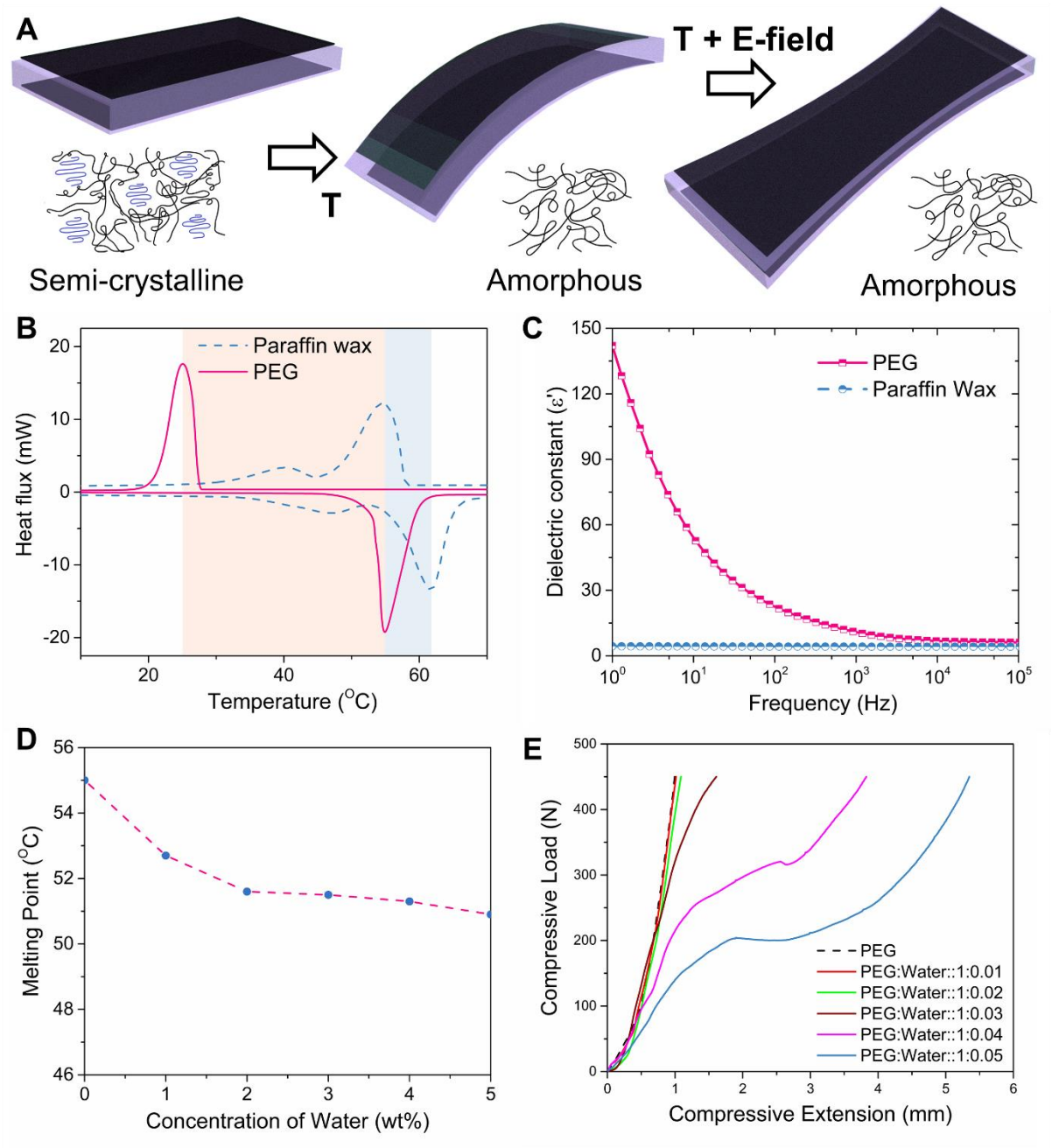

Figure 1. Design and Choice of materials. (A) Thermally activated phase transition from a semi-crystalline state to an amorphous state creates drastic variation in the mechanical properties, which in turn enables modulation of the force output from the composite. Thermally

activated phase transition can be coupled with electrically driven shape morphing. (B) DSC curves (2 cycles) for PEG (MW=2000) and paraffin wax showing melting and solidification behaviors. (C) Plot of dielectric constant against frequency for PEG (MW=2000) and paraffin wax, revealing higher dielectric constant values for PEG. (D) Plot of melting point of PEG-water mixture against varying concentration of water. As the water content increases, melting point decreases. (E) Uniaxial compression test of PEG and PEG-water mixtures. As the water content increases, there is a softening of the matrix and mechanical strength is compromised.

Based on the measured material properties, PEG emerges as a suitable choice for fabrication of reversible rigidity composites. However, the large operational temperature window for PEG translates to sluggish response times. To overcome this, it is desired to shift the melting and crystallization points closer to each other. Metal eutectics serve as an inspiration as they are two component system and addition of another component leads to reduction of melting point.[31] Previous reports have indicated that addition of water to PEG leads to formation of eutectic mixtures via hydrogen bonding without any change to the helical crystal structure of the PEG.[32,33] Hence, it is expected that addition of water would result in lowering of melting point of PEG. To this end, varying concentrations of water was added to PEG matrix to form different hypo-eutectic PEG-water mixtures. As the concentration of water increased from 0% to 5% (wt%), there was a corresponding decrease in the melting point from 55℃ to 50.9℃ (**Fig. 1D**). There was no significant change to the crystallization behaviour of PEG (**Fig. S4**). From the uniaxial compression test (**Fig. 1E**), it was evident that the increasing water concentration in the system leads to softening of the matrix and reduction of mechanical strength. Increasing the water concentration beyond 5% yielded samples with non-homogeneous mixture of solid and liquid phases.

To shift the crystallization point, deliberate addition of external nucleating agents to a polymer melt is a popular strategy for shifting from homogeneous to heterogeneous nucleation (**Fig. 2A**). MXenes are an emerging group of 2D materials with layered sheets of carbides and nitrides of transition metals, known for their superior properties like high electrical conductivity, thermal stability, hydrophilic nature and high thermal conductivity. Addition of

MXenes nanoflakes are expected to lower the free energy barrier of the PEG-water hypo-eutectic mixture by reducing the interfacial energy, moving the nucleation from homogeneous to heterogeneous (**Fig. 2A**). As purchased MXene ($Ti_3C_2T_X$) was intercalated with Li^+ ions for increasing the spacing between the layers (**Fig. 2B**) and suspension in DI water were prepared. Keeping the concentration of water fixed @ 3% (concentration chosen owing to significant change in melting point without change in mechanical properties), increasing the MXene concentration increases the crystallization temperature (**Fig. 2C**). Crystallization point increases from 25℃@ 0 mg/ml to 33.5℃ @ 10 mg/ml. 10 mg/ml concentration was chosen for the highest increase in the crystallization point. Interestingly, other ceramic and carbonaceous nanoparticles do not manage to show any significant effect on the crystallization point for similar concentrations. (**Fig. S5**) This can be attributed to high specific surface area and larger layer spacing of MXene nanosheets and physical adsorption between PEG and MXene owing to surface tension force and hydrogen bonding interactions. [34]

Overall, the operational temperature window for MXene incorporated PEG-water hybrids was reduced to 18℃ from 30℃ (for pristine PEG) (**Fig. 2D**). Water in the hybrid system shifts the melting in the DSC thermogram leftwards, bringing down the melting point (**Fig. 2D**). MXene nanoflakes in the mixture shifts the crystallization in the DSC thermogram rightwards, lifting up the crystallization point (**Fig. 2D**). This shift in the operational temperature window and rapid nucleation leads to faster crystallization of MXene incorporated PEG-water hybrids after melting. Where, pristine PEG displays homogeneous nucleation (**Fig. 2E**) with a limited number of nucleating sites, addition of MXene nanoflakes introduces several nucleating sites within the hybrid system melt, leading to heterogeneous nucleation (**Fig. 2F**). This reduces the overall cycle time for melting and crystallization by more than half, 300 seconds for MXene incorporated PEG-water hybrids as compared to 630 seconds for pristine PEG (Video S2).

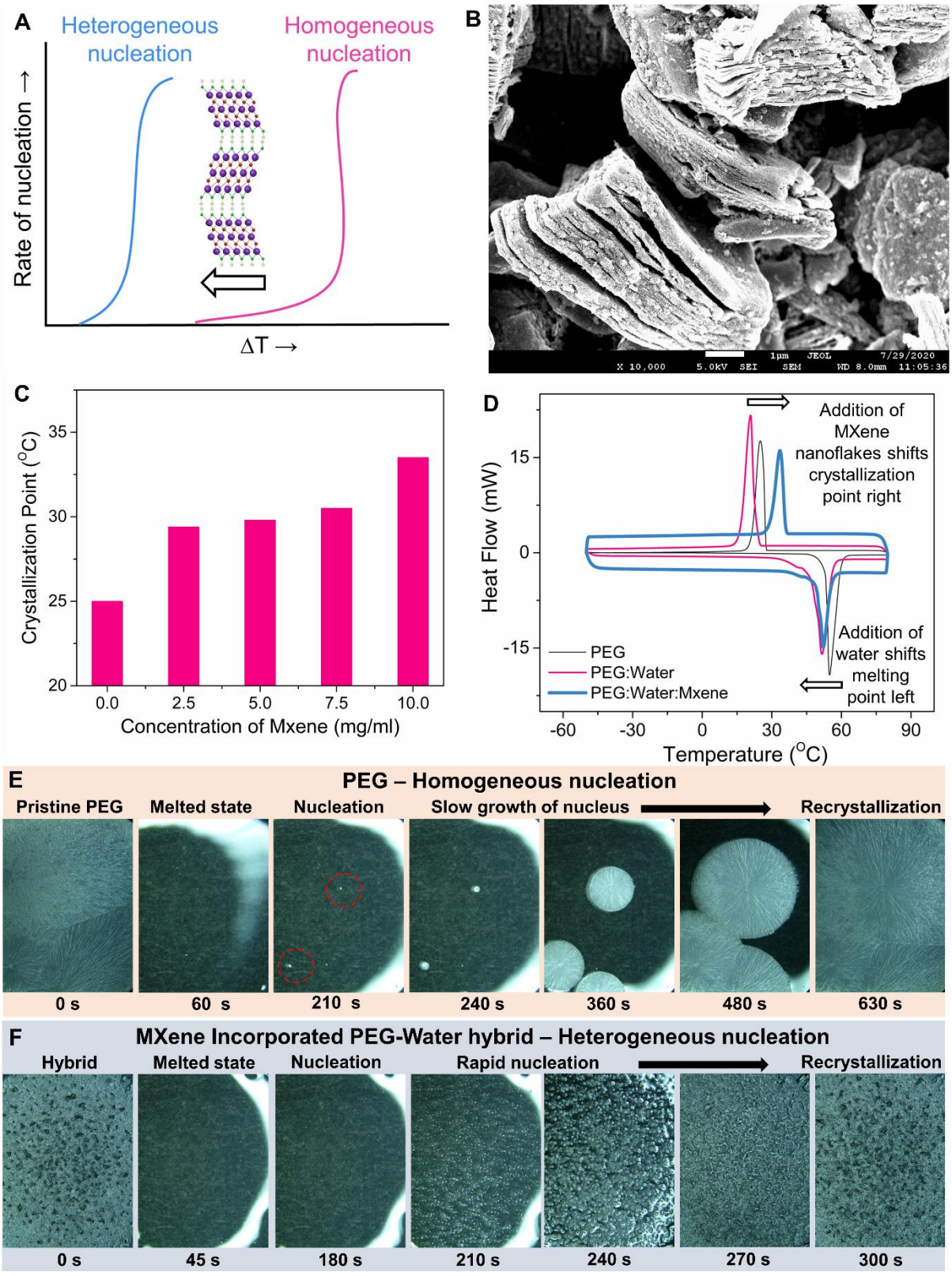

Figure 2. MXenes as nucleating agents for PEG-water mixtures. (A) Schematic of shifting from homogeneous nucleation to heterogeneous nucleation by addition of MXene nanoflakes as nucleating agents. (B) SEM (Scanning electron microscopy) image showing the layered structure of MXene nanoflakes (before exfoliation). (Scalebar – 1 μm) (C) Plot of variation in crystallization point against varying concentration of MXene nanoflakes. (D) DSC

thermograms for pristine PEG, PEG-water mixture (1:0.03) and MXene incorporated PEG-water hybrid (1:0.03 & MXene concentration in DI water = 10 mg/ml). Addition of water shifts the melting leftwards (decrease of melting point) and addition of MXene nanoflakes shifts the crystallization rightwards (increase of crystallization point), leading to reduction of operational temperature window. (E) Optical microscopy images of melting and crystallization of pristine PEG, showing slow and homogeneous nucleation process. Complete cycle takes 630 seconds. (Scalebar – 2.9 mm) (F) Optical microscopy images of melting and crystallization of MXene incorporated PEG-water hybrid, showing rapid and heterogeneous nucleation process. Complete cycle takes 300 seconds.

2.2 Rigidity modulation in phase change hybrids

Rigidity encompasses the ability of the material to resist mechanical deformation homogeneously and isotropically. [12,22] MXene incorporated PEG-water hybrids based bulk composites demonstrated the ability to modulate their flexibility based on thermal stimulus. In their rigid state (**Fig. 3A**), composites showed the ability to resist bending under load, with no visible deformation or deflection under the applied load of 1.25 N on either side. On thermal input, the hybrid transitioned to a soft state where it bent completely under its own load (**Fig. S6** & Video S3). In addition to its ability to modulate flexibility, the hybrid also demonstrated a significant difference of ~10 times in hardness between the rigid and the soft states. As shown in **Fig. 3B**, hardness measurement in the rigid state returned a value of ~50 Shore A compared to value of ~5 Shore A for the soft state of the hybrid (pristine PDMS = 35 Shore A hardness, **Fig. S7**). Another significant aspect of rigidity modulation is the ability to modulate stretchability. MXene incorporated PEG-water hybrids bulk composites demonstrated the capability to resist stretching, in their rigid state, when subjected to applied load (1N) with no visible stretching or deformation (**Fig. 3C**) in their rigid state. As the PEG is melted, bringing the composite to the soft state, it is able to easily stretch along the direction of the applied load (**Fig. 3C**) (Video S3). Temperature dependant 3-point bending test (**Fig. 3D**) provides information about flexural strength and flexural modulus of hybrid in its rigid and soft state. The load-deflection curve for the composite in its rigid state has a very steep slope compared to the soft state. Flexural strength and flexural modulus of the hybrid in rigid state were

calculated as 1.46 MPa and 202.6 MPa respectively, compared to 0.025 MPa and 2.13 MPa respectively for the composite in soft state indicating an impressive ~100 times modulation in flexural strength and flexural modulus (**Table 1**). Temperature dependant uniaxial tensile testing (**Fig. 3E**) was performed to quantify the modulation of Young's modulus and stress-strain behaviour of the MXene incorporated PEG-water hybrids in rigid and soft state. In its rigid state, hybrid has a very steep stress-strain curve, indicative of high mechanical stiffness with the Young's modulus calculated to be 6.23 MPa. On the other hand, in its soft state, the hybrid deforms without the application of any significant stress and the calculated Young's modulus was 7.87 kPa. A remarkable transition in the mechanical stiffness (Young's modulus) of ~700 times is thus recorded (**Table 1**).

Table 1. Table summarizing comparison of current work with other stiffness and rigidity modulation approaches. Different device and material configurations have been adopted, and hence a direct comparison between the results is not possible.

S. No.	Material system	Mechanism	Deformation mode	Parameters		Reference
1	Propylene-ethylene copolymer with structured carbon black	Glass transition	Tensile	Young's modulus @ non-activated state	10.4 MPa	Rich et. al. [35]
				Young's modulus @ activated state	0.7 MPa	
2	Field's metal embedded within an elastomer film	Melting	Tensile	Young's modulus @ non-activated state	0.86 GPa	Shan et. al. [36]
				Young's modulus @ activated state	95.2 kPa	
3	Iron crosslinked Sodium acrylate-Polyethylene glycol diacrylate hydrogels	Electroplastic transition	Compressive	Compressive modulus @ reduced state	0.6 MPa	Calvo-Marzal et. al. [37]
				Compressive modulus @ oxidised state	1 MPa	
4	Silicone foam impregnated with Field's metal	Melting	Tensile	Young's modulus @ non-activated state	1.8 MPa	Van Meerbeek et. al. [38]
				Young's modulus @ activated state	0.1 MPa	
			Compressive	Compressive modulus @ non-activated state	3.1 MPa	
				Compressive modulus @ activated state	0.1 MPa	

5	Propylene-ethylene copolymer with structured carbon black	Glass transition	Tensile	Young's modulus @ non-activated state	36.8 MPa	Shan et. al. [23]
				Young's modulus @ activated state	1.49 MPa	
6	Structured fabrics undergoing jamming phase transition	Jamming	Bending	Bending modulus @ non-activated state	~ 35 MPa	Wang et. al. [39]
				Bending modulus @ activated state	~ 1.4 MPa	
7	PEG-water-MXene hybrid	Melting	Tensile	Young's modulus @ non-activated state	6.23 MPa	Current work
				Young's modulus @ activated state	7.87 kPa	
			Flexure	Flexural modulus @ non-activated state	1.46 MPa	
				Flexural modulus @ activated state	0.025 MPa	
			Bending	Shore hardness @ non-activated state	~50 Shore A	
				Shore hardness @ activated state	~5 Shore A	

MXene incorporated PEG-water hybrid is brittle solid and it renders the system prone to fracture and damage from unexpected mechanical loading and high impact forces, unavoidable in practical scenarios. [27] However, owing to its ability to melt and solidify over several cycles, the material system imbibes the sample with the ability to heal after damage. Pristine samples were subjected to severe damage (as evident from the crack) and healed by melting and solidification (**Fig. 3F**). This cycle was repeated, and mechanical behaviour of the pristine and healed sample was studied by 3-point bending tests at each stage. As observed in **Fig. S8**, the sample maintains very similar load-extension curves even after 2 cycles of healing, and nearly identical slopes for the curves. Flexural modulus was calculated to be 205 MPa for fresh sample, which reduced to 196 MPa after 1st cycle of healing and increased to 222 MPa after 2nd cycle of healing. The slight difference in flexural modulus can be attributed to the variation of the solidification process for the bulk composite.

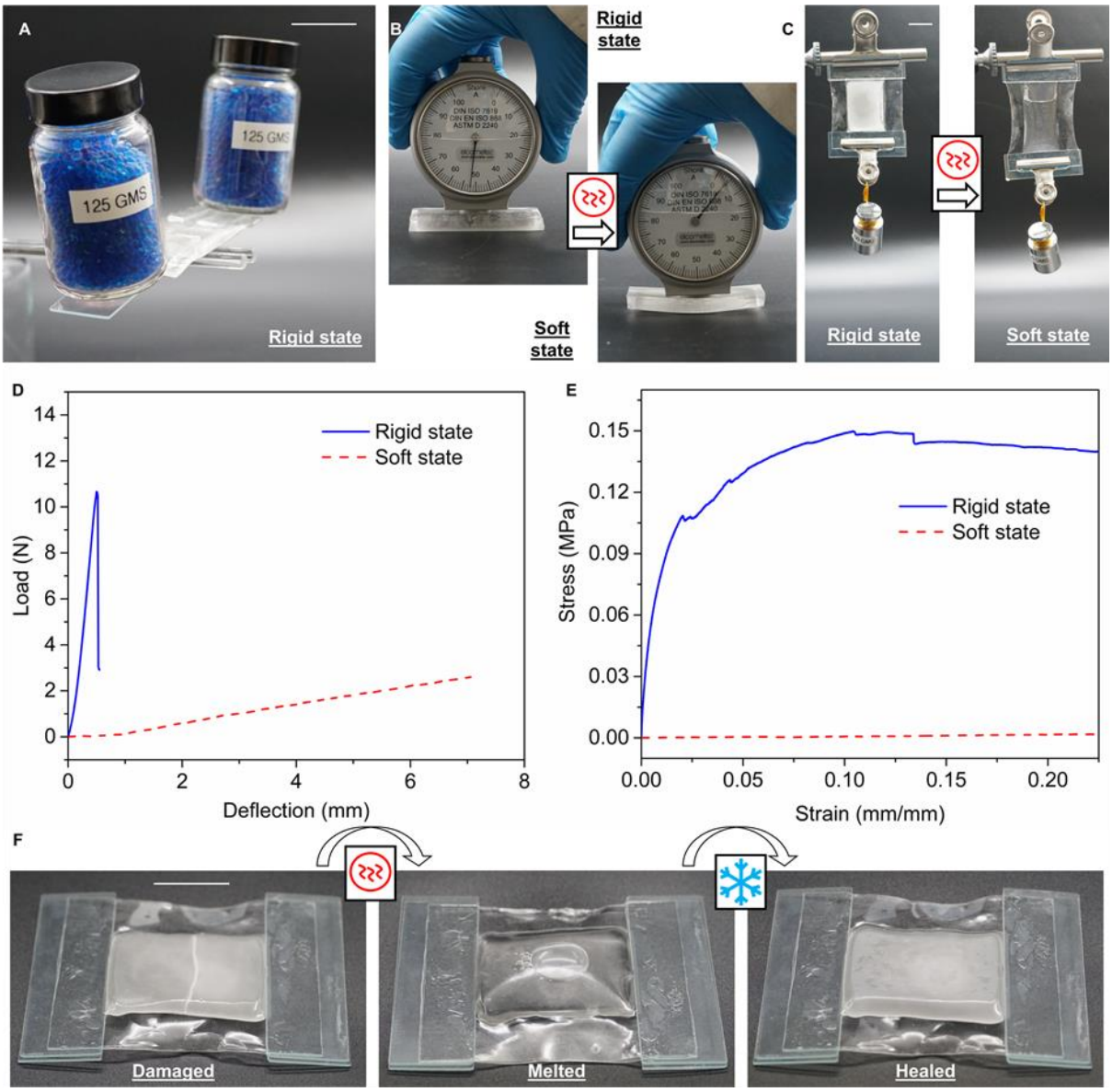

Figure 3. R**igidity modulation in MXene incorporated PEG-water hybrids.** (A) Demonstration of the flexural modulation of the sample where it resists bending under applied load in rigid state. (Scalebar – 2.5 cm) (B) Hardness measurement using a Shore durometer for rigid and soft state of the sample. (C) Demonstration of the ability of the sample to resist stretching under applied load in rigid state and allowing stretching in soft state. (Scalebar – 2.5 cm) (D) Load-deflection curve from temperature dependant 3-point flexural tests for hybrid in rigid state and soft state. (E) Stress strain curve for hybrid in rigid state and soft state obtained by temperature dependant uniaxial tensile tests. (F) MXene incorporated PEG-water hybrids can restore their structural integrity and mechanical strength upon fracture by healing via the process of melting and solidification. (Scalebar – 2.5 cm)

2.3 Thermoresponsive hybrids as electroactive layer in a DEA configuration

Owing to its attractive thermal, mechanical and dielectric properties, MXene incorporated PEG-water hybrids enable a single material system capable of thermally triggered modulation of mechanical properties and electrically controlled shape morphing. Having demonstrated the modulation of mechanical properties, we show the actuation behavior of hybrids in a DEA configuration. Electric field driven DEAs are known for their high efficiencies, light weight design and superior structural compliance. [19,20,40] DEAs are variable capacitors, in their simplest configuration, with an elastomeric dielectric sandwiched between compliant electrodes on either side (**Fig. 4A**). [19,20] When an electric field is applied across the electrodes, opposing charges on either side the membrane exerts electrostatic pressure on the film (attractive forces between opposing charges). This attractive force in the thickness direction results in reduction of the thickness of sandwiched membrane and resulting in the stretching out of the elastomer in areal direction (**Fig. 4A**). [19,20] The actuation strain produced is directly proportional to the dielectric constant of the elastomer and inversely proportional to the Young's modulus. [19-21] Similar to architecture of electrohydraulic soft actuators, we fabricate DEAs in which an elastomeric shell is filled with a dielectric fluid and sandwiched between compliant electrodes. [9,15,41] **Fig. 4B** shows the schematic of the actuator with an elastomeric shell filled with the PEG-water-MXene hybrid and compliant electrodes, overlapping each other, on either side. When an electric field is applied across the electrodes, the shell and the fluid experiences electrostatic pressure. Fluid has negligible resistance to deformation (for practical considerations, Young's modulus is zero) and gets displaced under the effect of this pressure, resulting in morphing of the elastomeric shell. [9,15] As expected, a quadratic relationship between linear actuation strain (measured at the centre of the actuator) and applied electric field was observed (**Fig. 4C**), because Maxwell stresses depend on square of the electric field applied. Owing to the high dielectric constant of PEG, an

actuation strain of ~28% was achieved at a low electric field of 0.9 V/µm. Actuation strain of 28% corresponds to ~2.5 mm depression (in actual terms) at the centre of the actuator (**Fig. S9**). The device demonstrates superior actuation performance compared to the state-of-the-art DEA devices, in a non-pre-stretched configuration with no external bias (dead weights, air pressure or magnetic field).[9,42,43] As observed from top and side view of the actuator (**Fig. 4D** & **Fig. 4E**), a huge visible deformation takes places at the centre of the actuator creating a shallow depression while the edges of the actuator deform to accommodate the displaced fluid volume. Furthermore, doping of PEG with water and MXene results in increased dielectric constant (**Fig. S10 A**). This could be attributed toa combination of dielectric behaviour of MXene-polymer interfaces under electric field and addition of small quantity of water to the matrix. MXene-polymer interfaces tend to form microscopic dipoles under the influence of an electric field and lead to charge accumulation, which in turn leads to a high dielectric constant.[44] Owing to the increased dielectric constant, improved actuation performance has been observed for PEG-water-MXene hybrids (~28% actuation strain @ 0.67 V/µm for PEG-water-MXene hybrid in comparison to 23% for pristine PEG) (**Fig. S10 B**). Such high actuation strain achieved at significantly low electric fields (**Table 2**) indicates the potential of utilizing MXene incorporated PEG-water hybrids as an active material for DEAs. Video S4 shows the dynamics of the actuator. One can visualize a use case scenario where electric field driven morphing of the elastomeric shell would be utilized to conform to an object and then the material solidifies around the object to keep it in place. This concept has been demonstrated by applying a thermal stimulus to the composite to change from rigid state to soft state. Once the composite reaches soft state, thermal stimulus was removed, and an electrical stimulus was applied to achieve shape-morphing. The composite was allowed to cool down naturally and reach rigid state in the morphed condition. (**Fig. S11** & Video S5)

Table 2. Comparison of actuation performance with other non-prestretched DEA configurations.

S. No.	Material system	Applied voltage	Electric field	Actuation strain	Reference
1	Hydraulically amplified self-healing electrostatic actuators	20 kV	NA	Thickness strain ~ 50%	Acome et. al.[9]
2	UV curable acrylates	3.75 kV	100-150 V/μm	Expansion - 22%; Contraction - 24%	Duduta et. al.[40]
3	Biaxially oriented polypropylene (BOPP) pouches filled with dielectric field	10 kV	240 V/μm	Longitudinal strain ~ 10%	Kellaris et. al.[15]
4	PUA–PEGDA copolymer films (15wt% PEGDA)	NA	24.2 V/μm	Areal strain ~ 50%	Tan et. al.[45]
5	PEG-water-MXene hybrids	5 kV	**0.67 V/μm**	Thickness strain ~ 28%	Current work

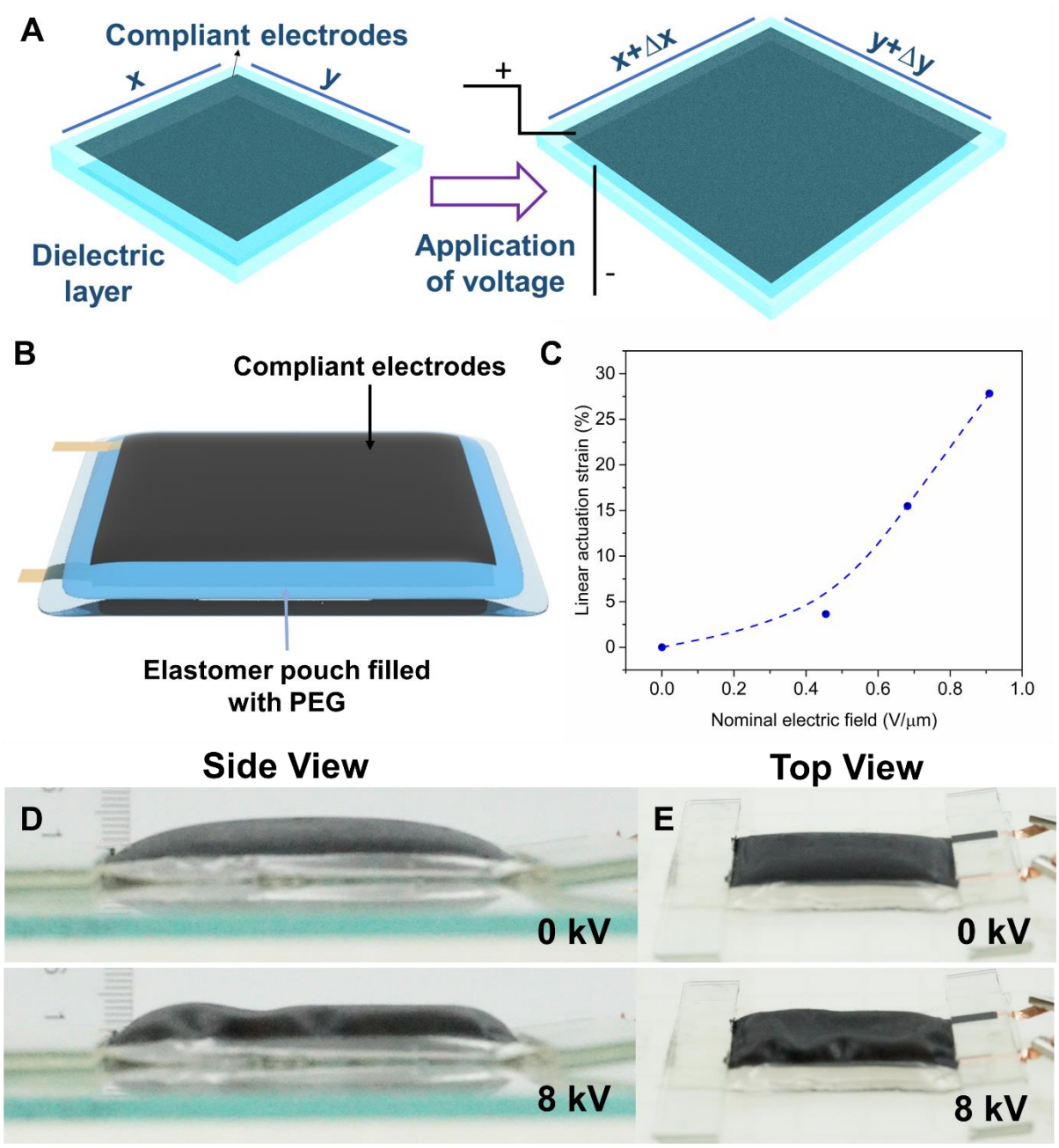

Figure 4. Surface modulation by utilizing as active layer in a DEA configuration. (A) Schematic showing DEA architecture with an elastomeric dielectric sandwiched between compliant electrodes on either side. Upon application of electric field, charges build up on the electrodes and the dielectric experiences electrostatic pressure along the thickness direction, originating from the electrostatic force. As a result of this, the elastomer stretches out in the plane to provide actuation. (B) Representative sketch of the proposed actuator, with an elastomeric shell filled with MXene incorporated PEG-water hybrids and covered with compliant electrodes on either side. (C) Plot of linear actuation strain, measured at the centre of the actuator, against the nominal electric field. Top (D) and Side (E) view of the actuator at 0 kV and 8 kV, showing the visible deformation taking place in the actuated state.

2.4 Programmable hardness modulation of surfaces via printing

Reversible melting and solidification of MXene incorporated PEG-water hybrids allows for printing on different substrates to create hardness domains (Video S6). Hybrid melt, printed on either rigid substrates (like glass) or flexible and stretchable substrates (elastomers like PDMS and acrylates), was able to maintain its shape during the solidification process and lines with a uniform width were obtained. Patterning of the hardness domains was performed through Direct-Ink-Writing (DIW) of the melted eutectic (**Fig. S12**). [46,47] Peano and Hilbert (**Fig. 5A**) fractal motifs, generally adopted for creating 2-dimensional conductive networks for stretchable and wearable electronics were printed (**Fig. S13**). [48] Pseudo 2D auxetic patterns (**Fig. 5A**) were also printed to demonstrate the versatility of the printing process and patterning of hardness domains. Arrays of patterns could be printed for creating large area and complex devices (**Fig. S14**). It is important to note here that due to brittle nature of PEG, stretching of the underlying elastomer resulted in cracking of patterns (**Fig. S15**). However, flexing of the samples, to a certain extent, was possible without damaging the patterns (**Fig. S16**).

Human-machine interaction necessitates development of surfaces with varying textures and form an important component of haptic information perceived by our receptors. [49] Changing the concentration of the functional component continuously across a pattern paves the way for achieving complex designs and imbibing regions with different surface textures. [50] These transitions in surface textures can be perceived by touch (as haptic information) when interacting with the interface and could be utilised to provide indications of new functionalities hidden below the surface, such as seamless integration of features like buttons beneath a surface. To achieve this functionally varying texture, methodical gradation of hardness (Video S6) was demonstrated via two deposition strategies.[50] Superposing new layers at specified geometrical locations on the underlying printed layer can create a gradient as illustrated by the varying step heights of the 3 different portions of the printed Peano curve (**Fig. 5A**). The next

strategy for printing a gradient of hardness was to vary the deposition rate, which leads to different quantity of material delivered along the deposition paths. 6 zigzag lines (**Fig. 5A**) were printed next to each other with increasing flow rates from 10 µl/min to 60 µl/min, in steps of 10 µl/min.

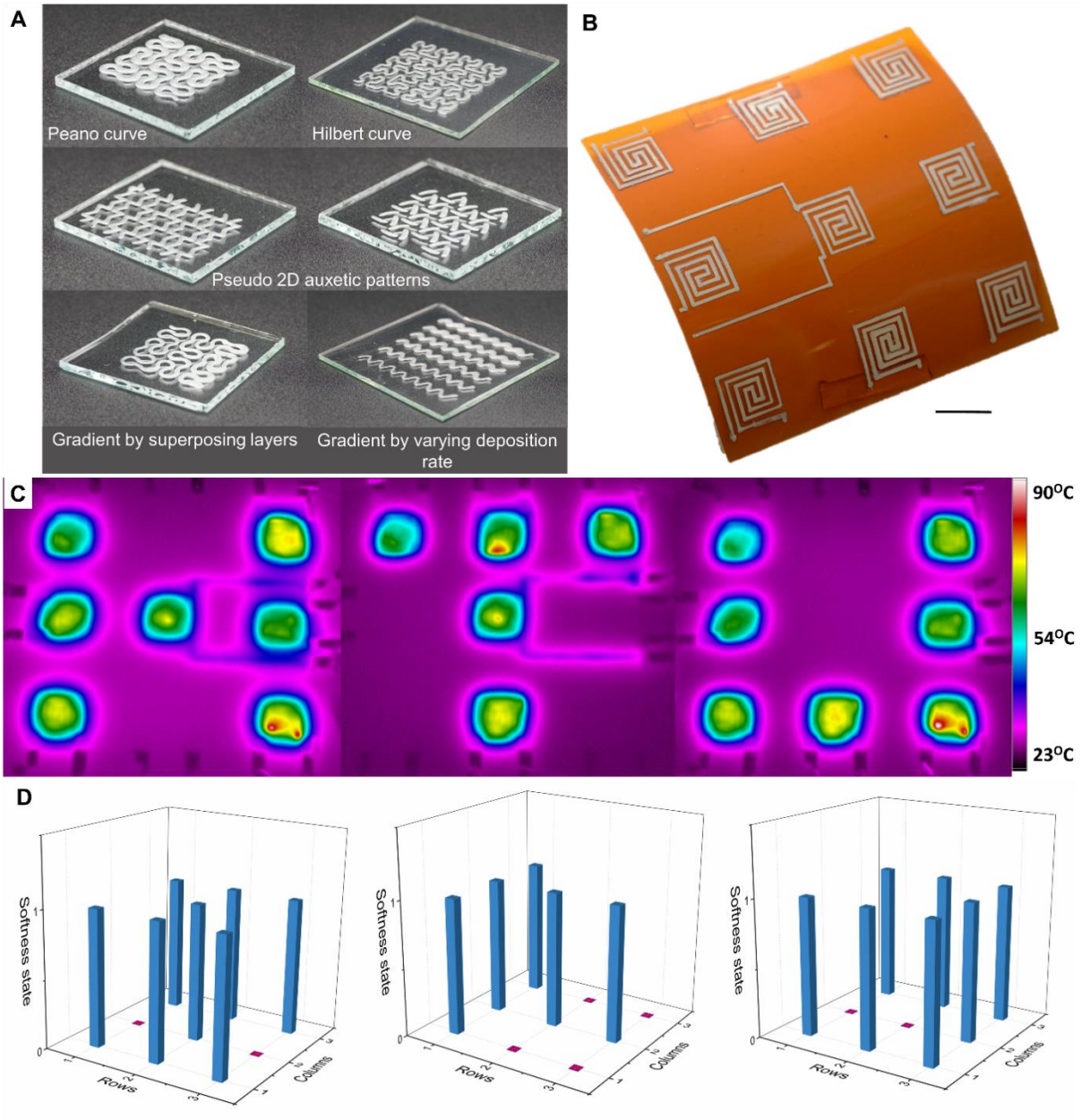

Figure 5. Programmable hardness modulation. (A) Printing of PEG-water-MXene hybrid into representative fractal motifs, Peano curve and Hilbert curve, and Pseudo auxetic patterns. Printing of the PEG-water-MXene hybrid allows to create hardness domains. Creating hardness gradients along the geometry of the Peano curve by deposition of superposing layers. Printing hardness gradients by varying flow rate of deposition along 6 equally spaced zigzag lines, in steps of 10 µl/min from 10 µl/min to 60 µl/min. (B) Image of an all-printed device for adaptive surface application fabricated on a flexible PI substrate. DIW printing of Ag paste is done on

the substrate in specific patterns, followed by the deposition of eutectic layer. Finally, the encapsulation layer of PDMS is printed on the top to cover the whole device. (C) Infrared camera images of three-by-three arrays of multiplexed devices after selective electrical trigger of different pixel combinations as the letters "N," "T" and "U". The changes in apparent temperature and thermal appearance are represented by changes in colour. (D) A hardness gradient is created by melting of eutectic at corresponding pixels, with regions with solidified eutectic at higher hardness values.

2.5 An all-printed device for adaptive surface application with controllable hardness modulation

Apart from passive textures on surfaces for enhanced human-machine interaction, adaptive surfaces that can modulate their properties will enable an immersive experience for the user in Virtual/Augmented reality applications. The ability of the MXene incorporated PEG-water hybrids to undergo dramatic changes in the mechanical properties allows it to be considered also as an active layer in adaptive surface applications. This is enabled by locally modulating the mechanical properties of the printed structures by incorporating printed joule heaters beneath them. The heaters fabricated by screen printing (**Fig. S17**) or through DIW (**Fig. S18**) have heating characteristics (**Fig. S19**, **Fig. S20** & **Fig. S21**) which indicate that temperatures far higher than melting point of MXene incorporated PEG-water hybrids are accessible at low voltages. No significant performance variation was noted under flexed condition (45 mm bending radius) (**Fig. S22**). The ability of the joule heaters to melt the hybrid was characterized (Video S1) by keeping a reference sample of bulk composite next to the sample with integrated screen-printed joule heater (**Fig. S23**) which confirmed the change in measured hardness. Subsequently, a 9-pixel device (3x3 array) was fabricated on a flexible PI substrate (**Fig. 5B**), with sequential printing of Ag patterns (joule heater) followed by deposition of MXene incorporated PEG-water hybrids (hardness domains) and PDMS (encapsulation layer) (cross-sectional schematic of device architecture shown in **Fig. S24**) (Video S7). The encapsulation helps the printed domain to retain their location and design after melting and crystallization cycles (**Fig. S24**). To begin with, the underlying MXene incorporated PEG-water hybrids

pixels below the PDMS encapsulation created hardness gradients within the device, owing to significant difference in Shore A hardness values for hybrid and PDMS. Individual patterns served as independently addressable "pixels". Ag heaters provided electrically controlled joule heating which can then be captured through thermal infrared imaging. The devices in the array displayed changes in their apparent temperatures upon device-specific and independent electrical trigger (Video S6) and allows different letters/patterns to be displayed (**Fig. 5C**). Heating leads to melting of MXene incorporated PEG-water hybrids deposited on top of the Ag heaters (Video S8), and this phase transition leads to a change of the hardness at corresponding pixels (**Fig. S25**, **Fig. S26, Fig. S27** & **Fig. S28**). Softness states corresponding to thermal patterns in **Fig. 5C** are presented in **Fig. 5D**. This hardness gradient created by soft and hard pixels can be perceived as haptic information. In principle, this fabrication approach can be readily amended to fabricate more complexed displays with higher pixel densities and finer pixel resolution. Higher pixel densities and finer resolution can enable new applications like camouflage platforms and wearable haptic communicators. [51,52] Furthermore, adopting transparent materials for the device architecture could also enable tunable optical devices and metasurfaces. [51,53]

3. Conclusion and Outlook

In the present work, we have introduced MXene incorporated PEG-water hybrids, which undergoes solid-to-liquid phase transitions upon application of thermal stimulus and allows for reversible modulation of mechanical properties. Intramolecular bonding, chain length, co-existence of crystalline and non-crystalline domains and presence of end hydroxyl groups in linear chain polymers like polyethylene glycol (PEG) allows for low melting point, high mechanical strength and high dielectric constant. However, significant temperature window between melting and solidification in the pristine polymeric system leads to sluggish reaction times. A hybrid system was architected to reduce this temperature window and improve cycle

times. Inspired by eutectic systems, water was added to PEG to form hypo-eutectic mixtures leading to reduction of the melting point. Addition of MXene nanoflakes provides multiple nucleating points by shifting towards a more heterogeneous nucleation. These approaches lead to rapid melting and crystallization of the hybrid mixture, reducing the reduction of the cycle time by more than half.

Reversible rigidity demonstrations were performed using the MXene incorporated PEG-water hybrids, with an impressive modulation of 700 times in Young's modulus, 100 times in flexural modulus and 10 times in hardness. These can be potentially utilized to create systems and surfaces which can modulate their behaviour on demand. Even after suffering critical structural damage, the hybrid system can be restored to its original state owing to the ability to melt and solidify over several cycles. Furthermore, owing to the favourable dielectric properties, the same thermoresponsive material system has been utilized as an electroactive layer for electric field driven DEAs. We demonstrated a peak linear actuation strain of ~28% at significantly low electric field of ~0.7 V/μm, a superior actuation performance compared to other state-of-the-art DEA devices.

Also, MXene incorporated PEG-water hybrids were exploited for patterning of hardness domains (demonstrated by printing of fractal motifs) and designing of hardness gradations by printing. This has, in fact, allowed for creating prototypical haptic devices, where printed hardness domains lead to creation of multimodal tactile information devices. Capitalizing on the printing of hardness domains, an all-printed device was fabricated for adaptive surface applications. A 3x3 array of pixels has been fabricated to demonstrate the capability of conveying tactile information by creating specific hardness gradients triggered by electrical actuation of individual pixels. Additionally, much complex haptic systems can be fabricated based on the printing strategy.

Beyond the applications demonstrated here, such a hybrid system could be potentially utilized in rehabilitative co-robots that can accommodate free motion of the patient in soft state and offer assistive mechanical work in rigid state. They could be used at the interfaces of exploratory robots capable of navigating a variety of terrains, like rocky terrain, easily deformable mud, or sandy beaches.

Materials and Methods

Material and Device fabrication and their characterization

Reversible stiffness composites were fabricated using 2 different elastomeric matrices; acrylates (3M VHB F9473PC, 250 microns) and PDMS (Dow Corning, Sylgard 184). For acrylate-based composite (**Fig. S29**), a rectangular area of VHB F9473PC tape, measuring 7.5 cm by 10 cm, was cut with the backing liner kept intact. Parafilm was cut and used as mask for brushing talcum powder on the elastomer. This is to prevent the internal elastomer region, where the pouch would be filled with phase-change filler, from sticking onto each other. Elastomer sheets are then folded along the dotted line and stick along the 3 edges after proper alignment. The borders are sealed owing to strong adhesive strength of these acrylic tapes. Phase-change filler (PEG) (Polyethylene glycol, Sigma Aldrich, MW = 2000) and Paraffin wax (Sigma Aldrich)) was first melted and then filled in the elastomer pouch by removing the backing paper from one side of the elastomer pouch. The elastomer is sealed from the 4th edge as well resulting in the fabricated elastomer pouch filled with phase-change filler. Thin acrylic elastomer contributes minimally to the overall stiffness of the composite. For silicone-based composites, the schematic for fabrication is shown in **Fig. S30**. A 3D printed mold was used for creating a PDMS elastomeric box (Length = 6 cm, width = 2 cm and height = 5 mm). It is then filled with the melted phase-change material and allowed to solidify. After solidification, another layer of PDMS is drop casted to seal the composite. MXene incorporated PEG-water hybrids were filled in the composites as required for demonstrations and characterisations.

For PEG-water composites, different quantity of DI water was added to PEG flakes. Then it was melted in an oven and mixed thoroughly using a vortex machine. PEG:Water::1:0.01 refers to 10 µl of water (10 mg) added to 1 gm of PEG. For PEG-water-MXene composites, different quantity of MXene-DI water suspension was added to PEG flakes. Then it was melted in an oven and mixed thoroughly using a vortex machine. $Ti_3C_2T_X$ HF-etched MXene was purchased from Laizhou Kai Kai Cermaic Materials Co. Ltd. (China). The powder was stirred in DMSO (Dimethyl sulfoxide, Sigma Aldrich) with LiBr (Lithium bromide, Sigma Aldrich) for 24 hours at 37℃ for intercalation. DMSO and LiBr were removed via solvent exchange process by washing with DI water several times (at 7-8℃). Required quantity of DI water was then added to create MXene dispersions with different concentrations. These dispersions were ultrasonicated (Ultrasonic cleaner, Fisher Scientific) (in ice bath) for 1 hour. 30 µl of these suspensions were added to 1 gm of PEG, which had different MXene concentrations. PEG-water-MXene hybrids appeared quite homogeneous and no phase separation of MXene nanoflakes were observed. (**Fig. S31**) This can be attributed to very low concentration of MXene in the hybrid and physical adsorption between PEG and MXene owing to surface tension force and hydrogen bonding interactions.

Thermal analysis was performed using DSC (TA Instruments, DSC Q10) and TGA (TA Instruments, TGA Q500). For a single DSC cycle, the temperature was ramped at 10℃/min from 0℃ to 100℃ and then ramped at 10℃/min from 100℃ to 0℃. For TGA, the temperature was again ramped at 10℃/min from 30℃ to 400℃. Acrylic tapes were used to create a mold for casting 2mm thick PEG and wax cuboids (3 cm by 3 cm) with no observable voids for performing the dielectric spectroscopy, performed on a dielectric spectrometer (Novocontrol, Alpha A analyser). Hardness measurements were done using a Shore durometer (ELCOMETER 3120). Tensile and compression tests were performed on a MTS C42 Universal test system, while 3-Point bending test was performed on Instron 5567 Universal test system.

Temperature dependant tensile and bending tests were done on a MTS C43 system with an integrated thermal chamber.

For analysing the actuation performance in a DEA configuration, an elastomeric shell (5.5 cm by 3 cm) was fabricated using acrylic tape (3M VHB F9473PC, 250 microns) and lower molecular weight PEG (MW=600) (6 ml) was utilized. Carbon grease electrodes were applied with a boundary of 7.5 mm on either side, defining the active area to be 5.5 cm by 1.5 cm. High voltage was applied to the actuator using a TREK MODEL 610E HIGH-VOLTAGE SUPPLY / AMPLIFIER / CONTROLLER. Vertical displacement was measured using a Keyence laser system (LK-H022K, Ultra-High-Speed/High-Accuracy Laser Displacement Sensor).

As procured silver (Ag) paste (Heraeus, SOL 327) was utilized for screen printing of joule heaters while it was diluted with butyl acetate (Sigma Aldrich) (5 gm Ag paste diluted with 5 ml butyl acetate) for direct-ink-writing. PDMS mixture prepared in 10:1 ratio (elastomer base: curing agent) was utilized for printing process.

For the 3x3 array of pixels, Arduino UNO was used to control the relays (SONGLE,SRD-05VDC-SL-C), which in turn regulated the input from power source (AIM TTi, MX100TP) to the individual pixels, which consisted of printed Ag electrodes (**Fig. S32**). These electrodes act up as Joule heater and they heat up current flows through them.

Direct-Ink-Write (DIW) printing

Zaber LSQ150A XYZ-stage with independent 3-axis motion system has been used to perform the DIW printing. In DIW, materials in their liquid-phase are deposited from a small nozzle under controlled flow rates, along the digitally defined paths to fabricate predesigned structures. The patterns were drawn in Inkscape. Using All to G-code converter, '.svg' files were converted to '.tap' files which are readable through notepad, and G-code coordinate values were generated. These coordinate values were then copied and pasted into the custom program, which was made using Python 3. Material feeding was done through syringe pump

(New Era, NE 1000) for MXene incorporated PEG-water hybrids and peristaltic pump (Masterflex L/S Standard Digital Pump Systems) for Ag paste and PDMS. Whilst the syringe pump was controlled directly through the program, peristaltic pump was controlled manually. Z-axis calibration was performed after placing the substrate to adjust the height of the tip. 18 Gauge needle tip was utilized, and the flow rate varied with the material system utilized (Ag paste = 700 – 800 µl/hour; MXene incorporated PEG-water hybrids = 10 µl/min (complex patterns, slow speed) to 45 µl/min (simpler patterns, fast speed); and PDMS = 40000 µl/hour).

Acknowledgments

The authors would like to acknowledge the funding support for this project from Ministry of Education (MOE) Tier 1 grant (MOE2018-T1-002-179) (Singapore). The project was partially supported by the NTU-SUG grant (9069) – Building blocks for next generation soft robots. We would like to thank N.S.N Ping (School of Materials Science and Engineering, Nanyang Technological University) for the access to Fluke thermal infrared camera. The authors would also like to acknowledge the support of Dr S.J.A. Koh (Robotic Materials, Max Planck Institute for Intelligent Systems) for providing access to the dielectric spectrometer.

CRediT authorship contribution statement

Ankit conceived the idea with the guidance from N.M. Ankit designed and led the research under the supervision of N.M., carried out the experiments, and analysed the experimental data. Ankit and F.K. fabricated the composite and actuators and performed their characterization. S.P. performed the Direct-Ink-Write of Ag, PEG and PDMS. S.P. prepared the MXene dispersions. K.J.R.L. prepared the screen-printed Ag heaters. M.R.K. helped in designing electrical circuit for all-printed haptic device. D.A. helped with mechanical characterization of bulk composites. Ankit & N.M. wrote the manuscript. All the authors contributed in reviewing the manuscript.

Competing interests

The authors declare that they have no known competing financial interests or personal relationships that could have appeared to influence the work reported in this paper.

References

1. Rus, D., and Tolley, M. T., Design, fabrication and control of soft robots, Nature, 521 (2015), 467.
2. Shen, Z., Zhu, X., Majidi, C., Gu, G., Cutaneous Ionogel Mechanoreceptors for Soft Machines, Physiological Sensing, and Amputee Prostheses, Adv. Mater., (2021), 2102069.
3. Ho, T. Y. K., Ankit, Febriansyah, B., Yantara, N., Pethe, S., Accoto, D., Pullarkat, S. A., Mathews, N., Inducing thermoreversible optical transitions in urethane-acrylate systems via ionic liquid incorporation for stretchable smart devices, J. Mater. Chem. A, 9 (23) (2021), 13615.
4. Shen, Z., Chen, F., Zhu, X., Yong, K.-T., Gu, G., Stimuli-responsive functional materials for soft robotics, J. Mater. Chem. B, 8 (39) (2020), 8972.
5. Accoto, D., Donadio, A., Yang, S., Ankit, Mathews, N., A Microfabricated Dual Slip-Pressure Sensor with Compliant Polymer-Liquid Metal Nanocomposite for Robotic Manipulation, Soft Rob., (2021).
6. Shepherd, R. F., Ilievski, F., Choi, W., Morin, S. A., Stokes, A. A., Mazzeo, A. D., Chen, X., Wang, M., Whitesides, G. M., Multigait soft robot, PNAS, 108 (51) (2011), 20400.
7. Hu, W., Lum, G. Z., Mastrangeli, M., Sitti, M., Small-scale soft-bodied robot with multimodal locomotion, Nature, 554 (7690) (2018), 81.
8. Bartlett, N. W., Tolley, M. T., Overvelde, J. T. B., Weaver, J. C., Mosadegh, B., Bertoldi, K., Whitesides, G. M., Wood, R. J., A 3D-printed, functionally graded soft robot powered by combustion, Science, 349 (6244) (2015), 161
9. Acome, E., Mitchell, S. K., Morrissey, T. G., Emmett, M. B., Benjamin, C., King, M., Radakovitz, M., Keplinger, C., Hydraulically amplified self-healing electrostatic actuators with muscle-like performance, Science, 359 (6371) (2018), 61
10. Sinkjaer, T., Toft, E., Andreassen, S., Hornemann, B. C., Muscle stiffness in human ankle dorsiflexors: intrinsic and reflex components, J. Neurophysiol., 60 (3) (1988), 1110.
11. Saavedra Flores, E. I., Friswell, M. I., Xia, Y., Variable stiffness biological and bio-inspired materials, J. Intell. Mater. Syst. Struct., 24 (5) (2013), 529.
12. Wang, L., Yang, Y., Chen, Y., Majidi, C., Iida, F., Askounis, E., Pei, Q., Controllable and reversible tuning of material rigidity for robot applications, Mater. Today, 21 (5) (2018), 563.
13. Aldred, N., Wills, T., Williams, D. N., Clare, A. S., Tensile and dynamic mechanical analysis of the distal portion of mussel *(Mytilus edulis)* byssal threads, J R Soc. Interface, 4 (17) (2007), 1159.
14. Mirvakili, S. M., Sim, D., Hunter, I. W., Langer, R., Actuation of untethered pneumatic artificial muscles and soft robots using magnetically induced liquid-to-gas phase transitions, Sci. Rob., 5 (41) (2020), eaaz4239.
15. Kellaris, N., Gopaluni Venkata, V., Smith, G. M., Mitchell, S. K., Keplinger, C., Peano-HASEL actuators: Muscle-mimetic, electrohydraulic transducers that linearly contract on activation, Sci. Rob., 3 (14) (2018), eaar3276.
16. Hu, W., Lum, G. Z., Mastrangeli, M., Sitti, M., Small-scale soft-bodied robot with multimodal locomotion, Nature, 554 (2018), 81.
17. Miriyev, A., Stack, K., Lipson, H., Soft material for soft actuators, Nat. Commun., 8 (1) (2017), 596.

18. Amend, J. R., Brown, E., Rodenberg, N., Jaeger, H. M., Lipson, H., A Positive Pressure Universal Gripper Based on the Jamming of Granular Material, IEEE Trans. Rob., 28 (2) (2012), 341.
19. Ankit, Tiwari, N., Rajput, M., Chien, N. A., Mathews, N., Highly Transparent and Integrable Surface Texture Change Device for Localized Tactile Feedback, Small, 14 (1) (2018), 1702312.
20. Pelrine, R., Kornbluh, R., Pei, Q., Joseph, J., High-Speed Electrically Actuated Elastomers with Strain Greater Than 100%, Science, 287 (5454) (2000), 836.
21. Ankit, Tiwari, N., Ho, F., Krisnadi, F., Kulkarni, M. R., Nguyen, L. L., Koh, S. J. A., Mathews, N., High-k, Ultrastretchable Self-Enclosed Ionic Liquid-Elastomer Composites for Soft Robotics and Flexible Electronics, ACS Appl. Mater. Interfaces, 12 (33) (2020), 37561.
22. Manti, M., Cacucciolo, V., Cianchetti, M., Stiffening in Soft Robotics: A Review of the State of the Art, IEEE Robot. Autom. Mag., 23 (3) (2016), 93.
23. Shan, W., Diller, S., Tutcuoglu, A., Majidi, C., Rigidity-tuning conductive elastomer, Smart Mater. Struct., 24 (6) (2015), 065001.
24. Cheng, N. G., Gopinath, A., Wang, L., Iagnemma, K., Hosoi, A. E., Thermally Tunable, Self-Healing Composites for Soft Robotic Applications, Macromol. Mater. Eng., 299 (11) (2014), 1279.
25. Shintake, J., Schubert, B., Rosset, S., Shea, H., Floreano, D., Variable stiffness actuator for soft robotics using dielectric elastomer and low-melting-point alloy. In *2015 IEEE/RSJ International Conference on Intelligent Robots and Systems (IROS)*, (2015), pp 1097.
26. Tonazzini, A., Mintchev, S., Schubert, B., Mazzolai, B., Shintake, J., Floreano, D., Variable Stiffness Fiber with Self-Healing Capability, Adv. Mater., 28 (46) (2016), 10142.
27. Sundararajan, S., Samui, A. B., Kulkarni, P. S., Versatility of polyethylene glycol (PEG) in designing solid–solid phase change materials (PCMs) for thermal management and their application to innovative technologies, J. Mater. Chem. A, 5 (35) (2017), 18379.
28. Lipton, J. I., Angle, S., Banai, R. E., Peretz, E., Lipson, H., Electrically Actuated Hydraulic Solids, Adv. Eng. Mater., 18 (10) (2016), 1710.
29. Sengwa, R. J., Kaur, K., Chaudhary, R., Dielectric properties of low molecular weight poly(ethylene glycol)s, Polym. Int., 49 (6) (2000), 599.
30. Koizuim, N., and Hanai, T., Dielectric Properties of Lower-membered Polyethylene Glycols at Low Frequencies, J. Phys. Chem., 60 (11) (1956), 1496.
31. Biloni, H., and Boettinger, W. J., CHAPTER 8 - SOLIDIFICATION. In *Physical Metallurgy (Fourth Edition)*, Cahn, R. W., and Haasen†, P., (eds.) North-Holland, Oxford, (1996), pp 669.
32. Huang, L., and Nishinari, K., Interaction between poly(ethylene glycol) and water as studied by differential scanning calorimetry, J. Polym. Sci., Part B: Polym. Phys., 39 (5) (2001), 496.
33. Graham, N. B., Zulfiqar, M., Nwachuku, N. E., Rashid, A., Interaction of poly(ethylene oxide) with solvents: 2. Water-poly(ethylene glycol), Polymer, 30 (3) (1989), 528.
34. Lu, X., Huang, H., Zhang, X., Lin, P., Huang, J., Sheng, X., Zhang, L., Qu, J.-p., Novel light-driven and electro-driven polyethylene glycol/two-dimensional MXene form-stable phase change material with enhanced thermal conductivity and electrical conductivity for thermal energy storage, Composites, Part B, 177 (2019), 107372.
35. Rich, S., Jang, S.-H., Park, Y.-L., Majidi, C., Liquid Metal-Conductive Thermoplastic Elastomer Integration for Low-Voltage Stiffness Tuning, Adv. Mater. Technol., 2 (12) (2017), 1700179.
36. Shan, W., Lu, T., Majidi, C., Soft-matter composites with electrically tunable elastic rigidity, Smart Mater. Struct., 22 (8) (2013), 085005.

37. Calvo-Marzal, P., Delaney, M. P., Auletta, J. T., Pan, T., Perri, N. M., Weiland, L. M., Waldeck, D. H., Clark, W. W., Meyer, T. Y., Manipulating Mechanical Properties with Electricity: Electroplastic Elastomer Hydrogels, ACS Macro Lett., 1 (1) (2012), 204.
38. Van Meerbeek, I. M., Mac Murray, B. C., Kim, J. W., Robinson, S. S., Zou, P. X., Silberstein, M. N., Shepherd, R. F., Morphing Metal and Elastomer Bicontinuous Foams for Reversible Stiffness, Shape Memory, and Self-Healing Soft Machines, Adv. Mater., 28 (14) (2016), 2801.
39. Wang, Y., Li, L., Hofmann, D., Andrade, J. E., Daraio, C., Structured fabrics with tunable mechanical properties, Nature, 596 (7871) (2021), 238
40. Duduta, M., Hajiesmaili, E., Zhao, H., Wood, R. J., Clarke, D. R., Realizing the potential of dielectric elastomer artificial muscles, PNAS, 116 (7) (2019), 2476.
41. Cacucciolo, V., Shintake, J., Kuwajima, Y., Maeda, S., Floreano, D., Shea, H., Stretchable pumps for soft machines, Nature, 572 (7770) (2019), 516
42. Vatankhah-Varnoosfaderani, M., Daniel, W. F. M., Zhushma, A. P., Li, Q., Morgan, B. J., Matyjaszewski, K., Armstrong, D. P., Spontak, R. J., Dobrynin, A. V., Sheiko, S. S., Bottlebrush Elastomers: A New Platform for Freestanding Electroactuation, Adv. Mater., 29 (2) (2017), 1604209.
43. Cao, C., Gao, X., Conn, A. T., A Magnetically Coupled Dielectric Elastomer Pump for Soft Robotics, Adv. Mater. Technol., 4 (8) (2019), 1900128.
44. Tu, S., Jiang, Q., Zhang, X., Alshareef, H. N., Large Dielectric Constant Enhancement in MXene Percolative Polymer Composites, ACS Nano, 12 (4) (2018), 3369
45. Tan, M. W. M., Thangavel, G., Lee, P. S., Enhancing dynamic actuation performance of dielectric elastomer actuators by tuning viscoelastic effects with polar crosslinking, NPG Asia Mater., 11 (1) (2019), 62.
46. Skylar-Scott, M. A., Gunasekaran, S., Lewis, J. A., Laser-assisted direct ink writing of planar and 3D metal architectures, PNAS, (2016), 201525131.
47. Ahn, B. Y., Duoss, E. B., Motala, M. J., Guo, X., Park, S.-I., Xiong, Y., Yoon, J., Nuzzo, R. G., Rogers, J. A., Lewis, J. A., Omnidirectional Printing of Flexible, Stretchable, and Spanning Silver Microelectrodes, Science, 323 (5921) (2009), 1590.
48. Fan, J. A., Yeo, W.-H., Su, Y., Hattori, Y., Lee, W., Jung, S.-Y., Zhang, Y., Liu, Z., Cheng, H., Falgout, L., Bajema, M., Coleman, T., Gregoire, D., Larsen, R. J., Huang, Y., Rogers, J. A., Fractal design concepts for stretchable electronics, Nat. Commun., 5 (1) (2014), 3266.
49. Culbertson, H., and Kuchenbecker, K. J., Importance of Matching Physical Friction, Hardness, and Texture in Creating Realistic Haptic Virtual Surfaces, IEEE Trans. Haptic, 10 (1) (2017), 63.
50. Giachini, P. A. G. S., Gupta, S. S., Wang, W., Wood, D., Yunusa, M., Baharlou, E., Sitti, M., Menges, A., Additive manufacturing of cellulose-based materials with continuous, multidirectional stiffness gradients, Sci. Adv., 6 (8) (2020), eaay0929.
51. Xu, C., Stiubianu, G. T., Gorodetsky, A. A., Adaptive infrared-reflecting systems inspired by cephalopods, Science, 359 (6383) (2018), 1495.
52. Besse, N., Rosset, S., Zarate, J. J., Shea, H., Flexible Active Skin: Large Reconfigurable Arrays of Individually Addressed Shape Memory Polymer Actuators, Adv. Mater. Technol., 2 (10) (2017), 1700102.
53. She, A., Zhang, S., Shian, S., Clarke, D. R., Capasso, F., Adaptive metalenses with simultaneous electrical control of focal length, astigmatism, and shift, Sci. Adv., 4 (2) (2018), eaap9957.